Small-Angle Neutron Scattering Study of Swollen Elongated Gels: Butterfly Patterns

E. Mendes,*,†,‡ R. Oeser,§ C. Hayes,†,§ F. Boué,|| and J. Bastide⊥,△

Ecole Supérieure de Physique et de Chimie Industrielles de la Ville de Paris, PCSM, Laboratoire associé au CNRS, URA 278, 10 rue Vauquelin, 75005 Paris, France, Institut Laue-Langevin, B.P. 156X, 38042 Grenoble Cedex, France, Laboratoire Léon Brillouin, CEN Saclay, 91191 Gif-sur-Yvette Cedex, France, and Institut Charles Sadron (CRM-EAHP), 6 rue Boussingault, 67083 Strasbourg Cedex, France

Received January 11, 1996; Revised Manuscript Received May 6, 1996[⊗]

ABSTRACT: Polymer gels swollen in a good solvent and subjected to a uniaxial deformation have been studied by small-angle neutron scattering (SANS). In all the experiments, the solvent is deuterated; this is equivalent to deuteration of the entire network. The gels were studied at two degrees of swelling, Q: $Q = 11$, which is very close to the preparation conditions ($Q_{prep} = 10$), and $Q = 23$, which is very close to the equilibrium degree of swelling in pure solvent, $Q_e = 24$. For each degree of swelling several elongation ratios ranging from 1.0 to 1.8 are investigated. For a fixed polymer concentration, it is shown that the scattered intensity at small angles in the direction parallel to the elongation axis increases with increasing deformation while it decreases in the perpendicular direction. Consequently, the isointensity curves mapped on a bidimensional detector are 8-shaped with a major axis parallel to the elongation direction. Such anomalous scattering contours, which cannot be explained by the classical theories of network deformation, are called "butterfly patterns". The experimental results are compared with the predictions of three recent models that account for butterfly isointensity curves in a SANS experiment of swollen elongated gels.

1. Introduction

Small-angle neutron scattering (SANS) is a powerful technique which probes correlations at molecular scales and, during the last two decades, it has been extensively used to study various problems in polymer science.[1] For example, consider the stress relaxation experiments performed on deformed melts.[2,3] In those early experiments, a mixture of deuterated and nondeuterated chains of the *same* molecular weight is deformed at a temperature above T_g, the glass transition temperature, and the system is quenched after different waiting times: the relaxation of the system can thus be followed by studying the scattering of the deuterated molecules. Information on the relaxation dynamics can easily be obtained by considering, for instance, the experimental scattering isointensity curves that are mapped on a bidimensional detector. The experimental results corresponding to the early stages of the relaxation process are in semiquantitative agreement with theoretical curves calculated according to the deformation assumptions of the reptation model:[4] the observed isointensity curves are ellipses, with major axis perpendicular to the elongation direction. The isointensity curves become more and more isotropic (circles) as the system relaxes. However, unexpected lozange shapes[5,6] were observed at intermediate times, but still with a major axis perpendicular to the stretching.

Even more unexpected results were obtained for mixtures of short deuterated chains and long nondeuterated chains for intermediate waiting times, t_w. For t_w greater than the Rouse relaxation time of the short chains but less than the longest relaxation time (reptation time) of the long chains: 8-shaped isointensity curves with major axis *parallel* to the elongation direction were observed.[7−9] These anomalous scattering patterns are known as *butterfly patterns*.

In fact, the butterfly patterns were first observed when studying the scattering from elongated cross-linked polydimethylsiloxane (PDMS) rubbers containing a fraction of free deuterated chains.[10] The length of the deuterated chains was comparable to the mesh size of the network. This effect was also found on a wide range of chain lengths for deuterated PS chains in PS networks. The main difference between the latter systems and the above-mentioned melts is the presence of cross-links in the nondeuterated chains. This implies an infinite final relaxation time since the chains forming the network cannot reptate. As in the case of melts, classical theories of rubber elasticity implicitly predict circular isointensity curves for uniaxially elongated networks containing free labeled relaxed chains.

SANS experiments using contrast variation methods performed on bimodal melts have shown that the butterfly patterns originate in the interchain structure factor. In the case of rubbers, this implies the existence of spatial concentration fluctuations in labeled free chains at scales which are larger than the mesh size of the system. One of the central hypotheses of classical molecular rubber theories is that they do *not* consider any correlation at scales which are larger than the mesh size.

Such an "homogeneity" hypothesis, on which the classical models are based, has recently been reconsidered.[11,12] It was argued that, under certain special conditions, the cross-linking process, though entirely random, could be responsible for the formation of large-scale spatial fluctuations in the elastic modulus ("hard zones" and "soft zones"). In practice, a model for heterogeneity formation in a polymer gel synthesized

* To whom all correspondence should be addressed.
† Ecole Supérieure de Physique et de Chimie Industrielles.
‡ Present address: Laboratoire d'Ultrasons et de Dynamique des Fluides Complexes, Unité de Recherche associée au CNRS no. 851, ULP, 4 rue Blaise Pascal, 67070 Strasbourg Cedex, France.
§ Institut Laue-Langevin.
|| Laboratoire Léon Brillouin.
⊥ Institut Charles Sadron.
△ Present address: Institut Curie, Section de Recherche, Physique et Chimie, 11 rue Pierre et Marie Curie, 75231 Paris Cedex 05, France.
⊗ Abstract published in *Advance ACS Abstracts,* June 15, 1996.

S0024-9297(96)00043-5 CCC: $12.00

by random cross-linking of a semidilute solution of long chains in a good solvent was considered. According to this model, the "hard zones" are expected to be branched, with a large distribution of sizes, and to grow in a completely screened fashion in the reaction bath. When the gel is subjected to a uniaxial elongation (the whole solvent being labeled with respect to the network), anisotropic spatial separation of hard zones amplifies the concentration fluctuations along the stretching direction, possibly generating butterfly patterns. Such an approach motivated us to make a preliminary SANS study of such deformed systems and, as predicted, butterfly patterns were actually observed in the small-angle scattering.[13,14] The difference between these systems and the above-mentioned PDMS rubbers or PS melts containing free labeled chains is that in the former a *good* solvent (small molecules) is used instead of a polymeric rather poor one (small free PDMS chains).

More recently, during the completion of the more extensive experimental study which we report in this paper, two new theories were developed in order to explain the butterfly patterns characteristic of elongated gels.[15−18] Contrary to the "cluster" model of frozen heterogeneities mentioned above, which is based on a fractal character of the random cross-linking (see next section), these new approaches are based on the elasticity theory. According to these models, thermodynamical concentration fluctuations[17,18] or thermodynamical *and* frozen concentration fluctuations[15,16] present in swollen gels could be responsible for the observation of butterfly patterns in a SANS experiment. Below, we compare the predictions of these two new models (namely the Onuki theory (refs 15 and 16) and the Rabin−Bruinsma theory (ref 18)), together with that of the "cluster model" (ref 12), with a set of data regarding gels prepared by random cross-linking of a semidilute solution, whose scattering properties have been studied both under swelling and under uniaxial extension.

As recalled above, the butterfly patterns are a common feature to the spectra of elongated gels, rubbers, and bimodal melts,[19] and it should be stressed that the data reported here can be considered as a part of a larger ensemble. The following experiments were indeed performed in parallel for seeking after the origin of the "butterfly patterns" in various systems: (i) SANS experiments on bimodal PS melts,[9] (ii) SANS experiments on PS networks containing free PS deuterated chains,[7,8] (iii) SANS experiments on uniaxially elongated polyacrylic acid gels,[20] (iv) coherent light scattering experiments, including speckle analysis, on gels made by end-linking.[21] More general discussions, summarizing the main features of the different series of results can be found in refs 22 and 23.

Finally, it must be stressed that a new theory of polymer gels, developed by Panyukov and Rabin,[24] has been published recently. Since that approach is quite recent, we could not include a comparison of its prediction with experiments in the present paper. It is the goal of a future publication.

2. Theories: A Brief Recall

In this section the basic ideas of the recent models which describe butterfly isointensity curves in elongated gels in a SANS experiment are recalled. The whole network is considered to be labeled with respect to the solvent. Three models are presented: (i) the *cluster model* which considers the scattering intensity as dominated by static spatial fluctuations of polymer concentration, related to clusterlike nonuniformities of the network structure,[12] (ii) the *Onuki theory*,[15,16] which takes into account both the thermal fluctuations in polymer concentration[25] *and* the static spatial fluctuations. Though based on a completely different formalism, this model can be considered, to some extent, as a generalization of model i which does not consider explicitly thermal concentration fluctuations. Finally, (iii) the *Rabin and Bruinsma theory*[18] in which a coupling between the strain field and *thermal* fluctuations of polymer concentration is proposed. Models ii and iii are both based on the elasticity theory formalism, but the hypotheses are considerably different in each of them.

2.1. The Cluster Model: Scattering from Frozen Concentration Fluctuations. Consider two identical systems A and B which are semidilute solutions of very long chains, with a polymer volume fraction equal to ϕ_{prep}. Each chain contains many "blobs", that is, the size of the chain is much larger than the screening length ξ_{prep}, which represents the size of the blob in the solution at ϕ_{prep}. Into one of the systems, say system A, cross-linking points are made at random very rapidly in such a way that the solution has no time to rearrange during cross-linking. In this case, effective cross-linking points would be those placed in the neighborhood of contact points between chains. At the same time, one assumes that the cross-links do not change considerably the concentration fluctuations in system A. This is equivalent to saying that the screening length of system A remains approximately the same as that of system B, that is, ξ_{prep}. The main difference between the two systems is that in system A some of the contact points cannot slip anymore. However, the small-angle neutron scattering from both systems would not be very different. This is effectively observed for sufficiently small cross-link concentrations.[14,26]

System A thus contains many blobs of size ξ_{prep}, with cross-link points at both extremities. They have been called "frozen blobs". Since tie-points are placed at random, frozen blobs will often be connected and will form regions richer in cross-links than on an average in the gel. Such clusters or hard zones, like percolation animals, are branched structures that may grow in a interspersed manner in the reaction bath.

If the same quantity of solvent is added to both systems A and B to give a new polymer volume fraction, ϕ, they will not behave identically. As regards system B, a semidilute solution, it is well known that dilution of the system will lead to a partial unscreening of the chains and a new correlation length $\xi_{sol} = \xi_{prep}(\phi/\phi_{prep})^{-3/4}$—or a new blob size—larger than the previous one, will be found.

In system A, hard zones richer in cross-link points are more difficult to deform than the gel on an average. Upon dilution of the system, the hard zones will separate from each other, leading to a distortion of the network. In the swollen state, the gel will present frozen concentration fluctuations that are not present in the semidilute solution. If the reticulation process is mapped into a percolation-of-blobs problem,[11] and for a system almost below the gelation threshold of blobs,[27] it is expected that $\xi_{gel} = \xi_{prep}(\phi/\phi_{prep})^{-5/3}$ (neglecting any stretching of the hard zones upon swelling). In this case, the screening length ξ_{gel} represents a kind of effective distance between undeformed hard zones. There is, in principle, a second unscreening process related to the dilution of soft interstitial zones, which

should behave as a semidilute solution. This is completely neglected in the derivation of the exponent: the only length scale considered in the system is ξ_{gel}.

In a scattering experiment, one can also determine by extrapolation the quantity $I(q \rightarrow 0)$, where q is the scattering vector amplitude. For both systems, gel and solution, the quantity $I(q \rightarrow 0)$ is expected to increase with dilution. In the case of solutions,[28] it is expected that $I_{sol}(q \rightarrow 0) \sim \phi^{-0.31}$, while for the statistical gel, with the approximations described above, it is predicted[11] that $I_{gel}(q \rightarrow 0) \sim \phi^{-5/3}$.

According to a similar interpretation,[12] when a gel is subjected to a uniaxial elongation, hard zones are anisotropically separated. In the direction parallel to elongation, as in the case of dilution, the intensity $I(q \rightarrow 0)$ will increase due to the unscreening of the correlations carried by hard zones. In the perpendicular direction, since the total volume of the system is conserved, the sample is macroscopically contracted and the screening of the correlations carried by the hard zones increases. Thus the scattering intensity at small-angles diminishes in this direction. Making a simple analogy between deformation and dilution and neglecting the stretching of the hard zones upon elongation (which is an oversimplification), it was proposed that the screening lengths in the parallel and perpendicular directions are given by[12]

$$\xi_{\parallel} = \xi\lambda^{\alpha_{\parallel}} \tag{1a}$$

$$\xi_{\perp} = \xi\lambda^{\alpha_{\perp}} \tag{1b}$$

with $\alpha_{\parallel} = 5$, $\alpha_{\perp} = -5/2$ and ξ is the value of the screening length for the isotropic state, which is not necessarily the preparation state. For a scattering vector **q** which makes an angle θ with the elongation axis, it is proposed that the screening length $\xi(\theta)$ varies as follows

$$\frac{1}{\xi(\theta)^2} = \frac{\cos^2\theta}{\xi_{\parallel}^2} + \frac{\sin^2\theta}{\xi_{\perp}^2} \tag{2}$$

and the intensity scattered at small-angles is written as

$$I(q,\theta) \approx \frac{\phi\xi(\theta)^{D_{eff}}}{1 + g(q,\theta)q^2\xi(\theta)^2} \tag{3}$$

where D_{eff} is an "effective" fractal exponent of hard zones ($D_{eff} = 8/5$). The crossover function, $g(q,\theta)$, should equal unity for $q\xi(\theta) \ll 1$. In the range $q\xi > 1$, where one probes essentially the interior of hard zones, the scattering intensity should be $I(q,\theta) \sim \phi q^{-8/5}$. Thus, it was postulated[12] that

$$g(q,\theta) \approx \frac{1}{1 + (q\xi(\theta))^{2-D_{eff}}} \tag{4}$$

The combination of eqs 2−4 gives isointensity curves in the form of butterfly patterns. From expression 3, we may write for the the intensity scattered at the limit $q \rightarrow 0$:

$$I(0)_{\parallel} = I(0)\lambda^{\beta_{\parallel}} \tag{5a}$$

$$I(0)_{\perp} = I(0)\lambda^{\beta_{\perp}} \tag{5b}$$

with $\beta_{\parallel} = 8$ for the parallel and $\beta_{\perp} = -4$ for the perpendicular direction. $I(0)$ is the intensity limit for isotropic conditions. The very strong absolute values for the exponents $\beta_{\parallel}$ and $\beta_{\perp}$ are a direct consequence of the strong simplification used in the model, that is, no stretching of hard zones is considered. Thus, observed exponents should be smaller than those predicted since the latter values correspond to limiting conditions.

It is important to stress that the exponents $\alpha_{\parallel}$, $\alpha_{\perp}$, $\beta_{\parallel}$, and $\beta_{\perp}$ are not independent. In the above approach, where only separation of the clusters is considered, $\alpha_{\parallel}D_{eff} = \beta_{\parallel}$, and $\alpha_{\perp}D_{eff} = \beta_{\perp}$ and, furthermore, $\alpha_{\perp} = -\alpha_{\parallel}/2$ and $\beta_{\perp} = -\beta_{\parallel}/2$.

2.2. Onuki's Model: Scattering from Thermal and Frozen Concentration Fluctuations. Thermal concentration fluctuations in polymer gels have been described by Tanaka *et al.*[25] and de Gennes.[28] Extending these approaches to elongated gels, Onuki[15,16] showed that such thermal fluctuations should be depressed in the direction of stretching. Therefore, one should not observe butterfly patterns with a major axis parallel to the elongation direction, but, on the contrary, butterfly patterns with a major axis perpendicular to the stretching direction. Such an orientation of butterflies, due to pure thermal concentration fluctuations, have not as yet been observed.

However, if frozen heterogeneities are present in the fluctuating elastic medium, butterfly patterns aligned along the elongation direction can be obtained by an elasticity theory approach.[15,16] In this case, the final intensity is given by a competition between thermal fluctuations and frozen concentration fluctuations. At small angles, the former tend to diminish the intensity scattered in the direction parallel to elongation while the latter tend to increase it.

Due to the rather heavy mathematics involved in the Onuki model, we will only recall the final results of the calculations.

In order to consider frozen concentration fluctuations, the cross-link density, ν_x, is allowed to fluctuate in space around its mean value ν with an amplitude $p \sim \langle(\delta\nu_x/\nu)^2\rangle$. In the limit of weak inhomogeneity, that is, $p \ll 1$, the scattering function at small angles of a gel swollen in a good solvent can be written as:

$$I(\mathbf{q}) = A\left(\frac{\phi^{5/3}}{\phi_x\phi_0^{2/3}}\right)\left[\frac{1}{\epsilon + J(\mathbf{q}) + C(\mathbf{q})q^2} + p^*\left(\frac{J(\mathbf{q}) - (\phi_0/\phi)^{-2/3}}{\epsilon + J(\mathbf{q}) + C(\mathbf{q})q^2}\right)^2\right] \tag{6}$$

The constant A permits comparison of the theoretical predictions with experimental data in absolute units (cm^{-1}), and it will be treated as an adjustable parameter. In expression 6, ϕ is the polymer volume fraction, ϕ_0 is the preparation concentration, ϕ_x is the average fraction of cross-link molecules per monomer unit ($\nu \sim \phi\phi_x$); ϵ is defined as $\epsilon = K_{os}/G + 1/3$, where K_{os} is the mean osmotic bulk modulus and G the mean shear modulus. The first term in the brackets corresponds to the contribution of the thermal concentration fluctuations alone, and the second to the contribution of frozen concentration fluctuations. $p^* = p(\phi_0/\phi)^{2/3}$; $C(\mathbf{q})$ is an unknown function of the scattering vector **q**. It was suggested[15,16] that $C(\mathbf{q}) \sim \xi^2$. $J(\mathbf{q})$ is a function of the elongation ratio λ, and it is given by

$$J(\mathbf{q}) = (\lambda^2 - \lambda^{-1})\cos^2\theta + \lambda^{-1} \tag{7}$$

with $\cos\theta = q_x/q$.

Actually, expression 6 may lead to butterfly isointensity curves in both directions, parallel or perpendicular, to the elongation axis. For a given gel, the strength of parameter p, that is, the degree of heterogeneity, determines the orientation of the isointensity curves. The larger the p, the larger the intensity scattered in the parallel direction when the gel is stretched. This intensity increase in the parallel direction is the signature of butterfly patterns with major axis aligned along the elongation axis. If the scattering from frozen heterogeneities is stronger than that from thermal fluctuations, butterflies are aligned along the parallel direction and *vice versa*.

In order to make a entirely quantitative comparison between theory and experiment, it is important to evaluate ϵ as a function of the polymer volume fraction, ϕ. In the approximation where the gel free energy density is written as a sum of a mixing free energy between polymer and solvent and an elastic term having a scaling form such as $\sim\phi^{1/3}$ (as in the James and Guth theory applied to gel swelling), the swelling pressure for a gel may be written as the sum of two independent terms[29]

$$\prod_{\text{gel}}(\phi) = \prod_{\text{mix}}(\phi) - G(\phi) \tag{8}$$

The first term, $\prod_{\text{mix}}(\phi)$, corresponds to the dilution of the polymer by the solvent, and it is usually comparable with the osmotic pressure of a semidilute solution. Thus, one writes $\prod_{\text{mix}}(\phi) = P_0\phi^{9/4}$, where P_0 is a positive constant, possibly lowered in gels with respect to solutions by about 30% (as shown by Horkay et al.[29] in the case of poly(vinylacetate) gels). The second term corresponds to the elastic shear modulus of the gel and avoids infinite dilution of the network. This term may also be written in a power-law form as $G(\phi) = G_0\phi^{1/3}$ with G_0 a positive constant.[30]

At equilibrium swelling in a pure solvent, that is, $\phi = \phi_e$, the swelling pressure of the gel vanishes and we can write $\prod_{\text{mix}}(\phi_e) = G(\phi_e)$. Thus, $P_0/G_0 = \phi_e^{-23/12}$. As the osmotic modulus is defined as $K_{\text{os}} = \phi\partial\prod_{\text{gel}}/\partial\phi$, using eq 8 we can write

$$\epsilon = \frac{9}{4}\left(\frac{\phi}{\phi_e}\right)^{23/12} \tag{9}$$

In reality, eq 8 is one form of the well-known additivity hypothesis for polymer gels and may be not rigorously valid.[31] However, the derivation of eq 6 makes use of this additivity. Thus, eq 9 does not introduce any new ingredient to the derivations of references 15 and 16.

At the limit $q \to 0$, expression 6 can be written

$$I_{\parallel}(0) = A\left(\frac{\phi^{5/3}}{\phi_x\phi_0^{2/3}}\right)\left[\frac{1}{\epsilon(\phi)+\lambda^2} + p^*\left(\frac{\lambda^2 - (\phi_0/\phi)^{-2/3}}{\epsilon(\phi)+\lambda^2}\right)^2\right] \tag{10a}$$

$$I_{\perp}(0) = A\left(\frac{\phi^{5/3}}{\phi_x\phi_0^{2/3}}\right)\left[\frac{1}{\epsilon(\phi)+\lambda^{-1}} + p^*\left(\frac{\lambda^{-1} - (\phi_0/\phi)^{-2/3}}{\epsilon(\phi)+\lambda^{-1}}\right)^2\right] \tag{10b}$$

for the scattering intensities in the parallel and perpendicular directions.

Consider now the dependence of the structure factor on the elongation ratio, λ, in the parallel and perpendicular directions. Expression 6 can be rewritten as

$$I_{\parallel}(\mathbf{q}) = A\left(\frac{\phi^{5/3}}{\phi_x\phi_0^{2/3}(\epsilon(\phi)+\lambda^2)}\right)\left[\frac{1}{1+\xi_{\parallel}^2\mathbf{q}^2} + \frac{p^*}{\epsilon(\phi)+\lambda^2}\left(\frac{\lambda^2 - (\phi_0/\phi)^{-2/3}}{1+\xi_{\parallel}^2\mathbf{q}^2}\right)^2\right] \tag{11a}$$

$$I_{\perp}(\mathbf{q}) = A\left(\frac{\phi^{5/3}}{\phi_x\phi_0^{2/3}(\epsilon(\phi)+\lambda^{-1})}\right)\left[\frac{1}{1+\xi_{\perp}^2\mathbf{q}^2} + \frac{p^*}{\epsilon(\phi)+\lambda^{-1}}\left(\frac{\lambda^{-1} - (\phi_0/\phi)^{-2/3}}{1+\xi_{\perp}^2\mathbf{q}^2}\right)^2\right] \tag{11b}$$

with

$$\xi_{\parallel}^2 = \frac{C(q)}{\epsilon(\phi)+\lambda^2}\,\xi_{\perp}^2 = \frac{C(q)}{\epsilon(\phi)+\lambda^{-1}} \tag{12}$$

In this approach, no theory accounts for the dependence of $C(q)$ on ϕ and λ.

2.3. Rabin−Bruinsma's Model: Scattering from Thermal Concentration Fluctuations Coupled to the Strain. In contrast to the "classical" thermal concentration fluctuations recalled in the last paragraph, Rabin and Bruinsma[18,31] have recently proposed a different mechanism that could be responsible for the observed butterfly patterns. They argue that structurally homogeneous elastic systems could present an anisotropic *modulation* of the thermal fluctuations along the elongation direction, when subjected to a uniaxial deformation. Such a modulation would be the result of a coupling between strain and thermal concentration fluctuations. In this section, we briefly recall the principal ideas of this model.

The problem is approched within the framework of a phenomenological Landau−Ginzburg theory which differs from other classical rubber elasticity theories through the existence of an internal degree of freedom. The considered as independent variables are the strain tensor, ϵ, the absolute temperature, T, and a scalar field, $\psi(r)$. The strain tensor is defined as

$$\epsilon_{ij}(r) = 1/2(\partial u_i/\partial r_j + \partial u_j/\partial r_i)$$

where the vector field $\mathbf{u}(\mathbf{r})$ is taken to be the continuum limit of the displacements of the positions $\mathbf{R}_i$ of the cross-links. Note that ϵ_{ij} should not be confounded with ϵ appearing in the preceding section. On macroscopic length scales, concentration is related to strain through an affine deformation assumption, and therefore, it is not a separate hydrodynamic variable. The internal field, $\psi(\mathbf{r})$, is defined as the relative change in the radius of the blob localized around the position $\mathbf{r}$, and it is responsible for the local liquidlike fluctuations of the internal structure of the gel. Both fields, strain and blob deformation, are coupled to the polymer volume fraction, ϕ, since any variation of one of those quantities leads to variations in the monomer concentration at length scales of the order of the mesh size.

The fluctuation in the free energy to the lowest order in amplitude is written as

$$\Delta F = \int\frac{d^3r}{2}\{2\mu(\psi)\epsilon_{ij}^2 + \lambda(\psi)\epsilon_{ij}^2 + 2C\epsilon_{ij}\psi + M(\nabla\psi)^2 + L(\nabla\epsilon_{ij})^2 + D\psi^2\}$$

where $\lambda(\psi)$ and $\mu(\psi)$ are the Lamé coefficients of an

isotropic gel, L is related to the correlation length of the system, D is the restoring modulus at a fixed specified strain, M is also related to the correlation length, ξ_ψ, of the blob size fluctuations, $\xi_\psi = (M/D)^{1/2}$, C is a coupling constant and $C = -D$.

The second difference between the present model and classical rubber theories is the fact that elastic constants may depend on internal degrees of freedom:

$$\lambda(\psi) = \lambda_g + (\partial\lambda/\partial\psi)_g\,\psi \quad \text{and} \quad \mu(\psi) = \mu_g + (\partial\mu/\partial\psi)_g\psi$$

with both $(\partial\mu/\partial\psi)_g$ and $(\partial\lambda/\partial\psi)_g < 0$.

For a uniaxial deformation in the **z**-direction, the strain tensor, in the limit of small deformation, is written, that is, $\epsilon = \lambda - 1$. The fluctuation spectrum is determined by expanding ΔF to second order in the Fourier components of the fluctuating fields followed by minimization with respect to ψ. They found the following expression for the structure factor

$$S(\mathbf{q}) = \frac{k_B T\phi^2}{E + L_S q^2 - \gamma\left(\dfrac{3q\mathbf{z}^2}{q^2} - 1\right)} \tag{13}$$

where $q^2 = q_x^2 + q_y^2 + q_z^2$, k_B, the Boltzmann constant, T, the absolute temperature, $\gamma = 2\epsilon(C/D)(\partial\mu/\partial\psi)$, $E = k_{os} + 4/3G$. $L_S = L' + 2\Gamma R_f^2 CE'/D$, with $L' = L + M(C/D)^2$, $E' = \lambda_g + \mu_g - C^2/D$, R_f is the Flory radius of the relaxed mesh and Γ a numerical constant.

Following the same procedure as in the preceding section, one can write

$$E = G_0(2.25\phi_e^{-23/12}\phi^{2,25} + \phi^{1/3}) = G_0 f(\phi) \tag{14a}$$

Up to now, no theory accounts for the dependence of the constant γ on polymer volume fraction. However, since $\gamma \sim \epsilon$, one can write:

$$\gamma' = \gamma(G_0 f(\phi))^{-1} = a(\phi) f(\phi)^{-1}(\lambda - 1) \tag{14b}$$

where $a(\phi)$ is a constant which depends, in principle, on polymer volume fraction, ϕ. Note, however, that $(C/D)(\partial\mu/\partial\psi) > 0$, and therefore, $a(\phi) > 0$. Expression 13 can be explicitly written for the intensity in the parallel and perpendicular directions.

$$I_\perp(q) = \frac{I_\perp(0)}{1 + \xi(\phi)_\perp^2 q^2} \tag{15a}$$

$$I_\parallel(q) = \frac{I_\parallel(0)}{1 + \xi(\phi)_\parallel^2 q^2} \tag{15b}$$

where

$$I_\parallel(0) = \frac{C_0\phi^2}{f(\phi)}\,\frac{1}{1 - 2a(\phi)f(\phi)^{-1}(\lambda - 1)} \tag{16a}$$

$$I_\perp(0) = \frac{C_0\phi^2}{f(\phi)}\,\frac{1}{1 + a(\phi)f(\phi)^{-1}(\lambda - 1)} \tag{16b}$$

and

$$\xi_\parallel = \xi(\phi)\left(1 - \frac{2a(\phi)(\lambda - 1)}{f(\phi)}\right)^{-1/2} \tag{17a}$$

$$\xi_\perp = \xi(\phi)\left(1 + \frac{a(\phi)(\lambda - 1)}{f(\phi)}\right)^{-1/2} \tag{17b}$$

In the above expressions, $\xi(\phi) = L_s/G_0 f(\phi)$, a complicated function of ϕ. We will take C_0 = constant x $k_B T G_0^{-1}$ as an adjustable parameter. Equations 15 show that the scattering intensity in the parallel and perpendicular directions can be written in a Ornstein–Zernicke form, with different effective correlation lengths. For positive values of the dimensionless strain, γ, the scattering intensity is suppressed in the perpendicular direction and it increases in the parallel direction. In this approach, this anisotropic increase of the scattered intensity is responsible for the formation of the butterfly patterns aligned along the elongation direction.

Rabin and Bruinsma[18,31] interpreted the above results as the formation, under strain, of a dynamical modulation of concentration. They suggest that dynamical "stripes" of different concentrations are formed in the system, in the direction perpendicular to the elongation axis.

3. Experimental Section

Samples. The gels were prepared by randomly cross-linking a semidilute solution using a Friedel–Crafts reaction described elsewhere.[32] Polystyrene chains of molecular weight $M_w \sim 700000$ ($M_w/M_n \sim 1.2$), were dissolved in 1,2-dichloroethane at a polymer volume fraction of $\phi = 0.1$. 1,4-Bis-(chloromethyl)benzene at a concentration of 0.8% mol/mol of monomer was used as a cross-linking agent, and the coreactor was $SnCl_4$ present at a concentration of 2% mol/mol of monomer. The mixture was heated at 60 °C for two days. Washing in tetrahydrofuran revealed a sol fraction less than 0.2%. Samples were then dried, polished (final dimensions $\sim$ 5.0 × 2.2 × 0.1 cm), and reswollen in deuterated commercial toluene (Aldrich, toluene-d_8, 99%) to two different swelling degrees, $Q = 12$ and $Q = 23$, with respect to the dried state. Samples were then placed in a quartz-windowed air-tight cell specially designed for the experiment. This cell permits sample elongation to the desired stretching ratio from the outside. During the experiment, the sample remained at equilibrium with the vapor pressure of the solvent. The elongation ratio λ varies from 1.0 to 1.85 ± 0.1.

SANS Experiments. The SANS experiments were performed at the Institut Laue-Langevin (ILL), Grenoble, using spectrometers D11 and D17. The spectrometer configurations were the following: incident wavelength, 10 Å (D11) and 16 Å (D17), and sample–detector distance equal to 10.0 m (D11) and 3.2 m (D17).

Data Treatment. Data were treated following the usual procedure using ILL software, that is, normalization of the detector using the flat incoherent scattering of water, masking the beam stop area and subtracting the contribution of the empty cell and the incoherent part of the signal. This latter was measured on separate background samples, bulk polystyrene and deuterated toluene. The intensity in the parallel and perpendicular directions was obtained by grouping data in circular sectors of 10°.

As will be seen in the following section, we use a screening length ξ for the gel, which was determined in analogy with semidilute solutions, by fitting the data at very low q to an Ornstein–Zernicke form ($I(q) = 1/(1 + \xi^2 q^2)$). ξ changes strongly with elongation ratio, especially in the parallel direction. In particular, for strong elongation ratios, the typical wave vector amplitude associated with ξ ($q^* = 1/\xi$) reaches very small q values. For such q's, it is well known that sufficiently concentrated solutions of long chains present an abnormal intensity scattering excess at small-angles, the so-called Picot–Benoît effect.[33] At very small values of q, this anomalous scattering excess may partly mask the Ornstein–Zernicke form of the semidilute solution scattering function. Since the gels used here are synthesized from the reticulation of semidilute solutions of very long chains, the excess scattering

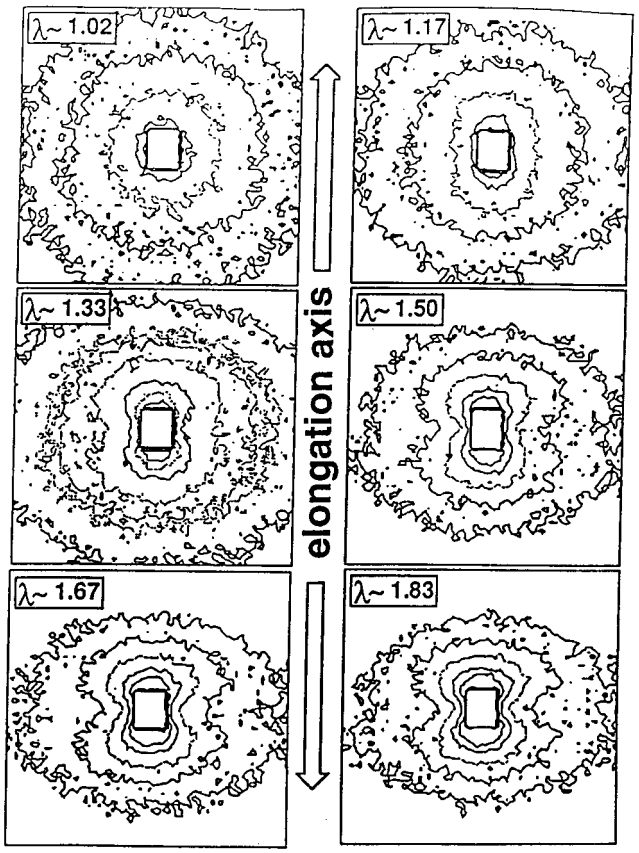

Figure 1. Isointensity curves as a function of the elongation ratio, λ, for the sample at swelling ratio $Q = 12$.

present in the solution *before* reticulation is frozen by the cross-linking process and it is also found in the scattering spectra of the gels. In order to achieve a higher precision in the measurement of ξ, the contribution of this abnormal scattering was subtracted from the spectra of the elongated gels following reference 21. This was possible because, in the present case, such a low q upturn does not depend significantly on the elongation ratio. The scattering spectra from which the low q upturn was subtracted were then fitted to the Ornstein−Zernicke function in order to determine the correlation length ξ and $I(q \rightarrow 0)$ for the different values of the elongation ratio λ.

In the Onuki theory, the scattering function is rather different from an Ornstein−Zernicke function: it is written as the sum of a Lorentzian and a squared Lorentzian. However, fitting data at very low q's with a squared Lorentzian gives almost the same value (within a few percent) for $I(q \rightarrow 0)$ as that found by fitting to a Lorentzian. Thus, for conciseness, we kept only the Lorentzian fit of $I(q \rightarrow 0)$ for discussing all the model predictions. The correlation length, which depends on the detailed expression of the scattering function is not discussed in the Onuki theory.

4. Results

In this section we present the results of the anisotropic scattering functions for swollen elongated gels. Two swelling ratios were studied: $Q = 12$, which is very close to the preparation state ($Q_0 = 10$) and $Q = 23$, which is very close to the equilibrium value in pure solvent ($Q_e \sim 24$). In Figure 1, the observed SANS isointensity curves are plotted as a function of the elongation ratio $\lambda = L/L_0$, for a swelling ratio $Q = 12$. Consider the higher values of the scattering vector **q** (outermost isointensity lines). For all the values of the elongation ratio (except $\lambda = 1.02$, which is almost isotropic), the isointensity lines are approximately ellipses, with the major axis aligned along the perpendicular direction.

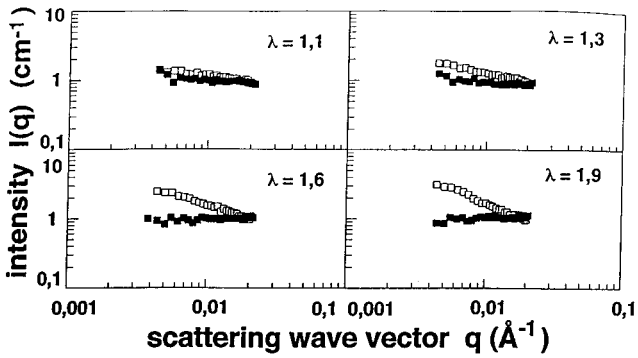

Figure 2. Scattered intensity $I(q)$ in the parallel (q) and in the perpendicular (n) directions as a function of q, for different elongation ratios, λ. A log−log representation is used. The swelling ratio is $Q = 12$.

The stronger the elongation ratio, the stronger the anisotropy. At these values of the scattering vector, distances comparable with the separation of cross-links are essentially probed. On such length scales, the stretching of individual chains, which are, on average, oriented along the stretching axis, is detected. Therefore, at these values of the scattering vector, the major axis of the isointensity curves is perpendicular to the stretching direction.

For smaller values of the scattering vectors, and even for small values of the elongation ratio, such as $\lambda = 1.17$, an important anisotropy is already detected, but in the *other* direction the isointensity curves have their major axis aligned *along* the elongation direction. For elongation ratios greater than $\lambda = 1.33$, the innermost isointensity contours begin to change shape and the *butterfly patterns* become more and more defined as the elongation ratio increases.

In order to characterize such an anisotropy, the scattered intensity in the parallel and perpendicular directions is plotted as a function of q in Figure 2, for different elongation ratios. Such curves are obtained after the data treatement described in section 3. In the plotted q range, the larger the elongation ratio, the larger the intensity scattered in the parallel direction. In the perpendicular direction, the opposite is observed: the intensity in the perpendicular direction decreases as the elongation increases.

The same sample has also been swollen to $Q = 23$, a swelling ratio very close to the maximum equilibrium degree of sweling ($Q_e \sim 24$). Qualitatively, as shown in Figure 3, the same behavior as for the preceding swelling ratio is found. Butterfly patterns aligned along the parallel direction are observed. Furthermore, as in the previous case, the stronger the elongation ratio, the stronger the butterfly pattern at smaller angles. For higher values of the scattering vectors the isointensity curves show a clear tendency to become ellipses. This again is related to the average stretching of individual chains. Note, however, that the q range corresponding to this Figure is shifted to smaller values of q with respect to Figure 1. Hence, the ellipses at higher q values are not as prominent as in Figure 1.

In Figure 4, the scattered intensity in the parallel and perpendicular directions is plotted for the sample swollen to $Q = 23$. The intensity scattered in the parallel direction increases strongly with λ while that in the perpendicular direction decreases. Such a decrease in the perpendicular direction is slighty larger than that of the preceding case ($Q = 12$).

From the scattered intensities in the parallel and perpendicular directions, it is possible to determine a

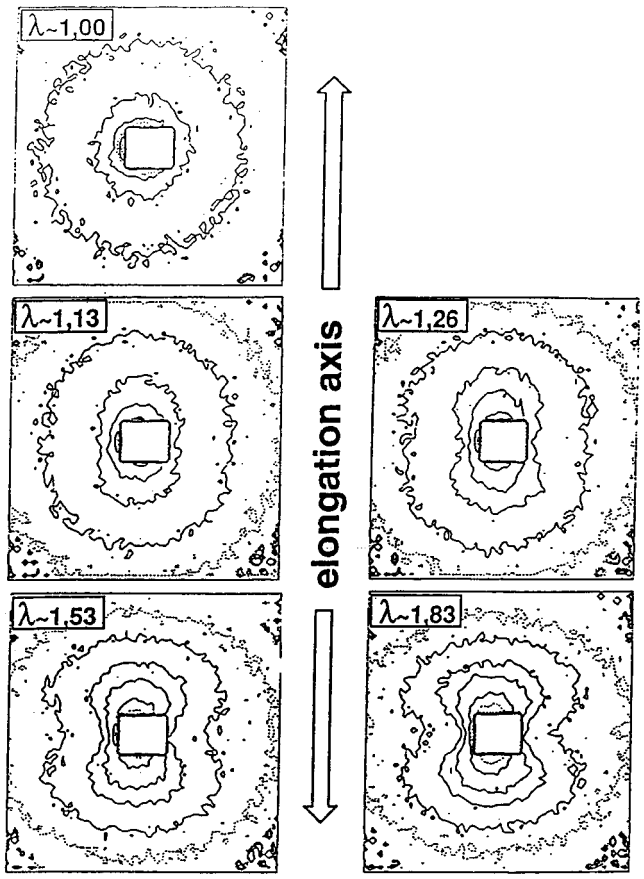

Figure 3. Isointensity curves as a function of the elongation ratio, λ, for the sample at swelling ratio $Q = 23$.

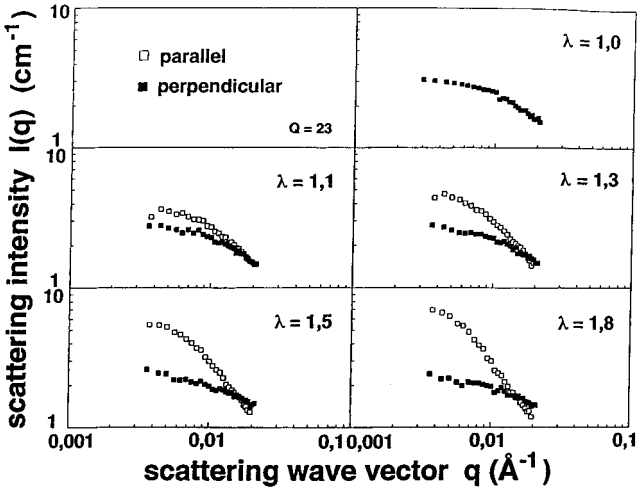

Figure 4. Scattered intensity, $I(q)$ in the parallel and in the perpendicular directions as a function of q, for different elongation ratios, λ. A log−log representation is used. The swelling ratio is $Q = 23$.

correlation length, ξ, and an extrapolated intensity, $I(q \rightarrow 0)$ (see paragraph 3). The values of ξ and $I(q \rightarrow 0)$, for a given elongation ratio, λ, are listed in Table 1, for both swelling ratios studied.

5. Discussion

Consider the shape of the observed isointensity curves at smaller q values. Qualitatively, all models recalled in paragraph 2 produce isointensity curves very similar to those observed, with butterfly patterns that develop with increasing elongation. Rather than making a quantitative comparison of the measured isointensity curves with those described by the theories, it is reasonable to compare the intensity scattered in the parallel and in the perpendicular directions.

Table 1. Scattered Intensity Extrapolated to Zero Scattering Vector, $I(q \rightarrow 0)$, and the Screening Length, ξ, Determined for the Parallel and Perpendicular Directions as a Function of the Elongation Ratio, λ

$Q = 12$			$Q = 23$		
λ	$I(q \rightarrow 0)_{\parallel}$	$I(q \rightarrow 0)_{\perp}$	λ	$I(q \rightarrow 0)_{\parallel}$	$I(q \rightarrow 0)_{\perp}$
1.0	1.3	1.3	1.0	2.86	2.86
1.1	1.34	1.02	1.13	3.92	2.76
1.3	1.68	0.93	1.26	4.4	2.43
1.6	2.98	1.02	1.53	6.59	2.3
1.88	4.43	0.97	1.83	9.34	2.22
λ	$\xi_{\parallel}$	$\xi_{\perp}$	λ	$\xi_{\parallel}$	$\xi_{\perp}$
1.0	18.6	18.6	1.0	49.0	49.0
1.1	37.2	17.7	1.13	66.3	45.9
1.3	53.6	12.5	1.26	89.3	41.8
1.6	93.1	11.9	1.53	103.2	38.8
1.88	134.9	10.1	1.83	140.4	52.6

Since we did not investigate the scattering from a gel *exactly* at the preparation concentration, we will first consider the dependence of the scattering from the polymer in the relaxed state, $\lambda = 1$, on the polymer volume fraction, ϕ. This first step tests the dependence of $I(q \rightarrow 0)$ on ϕ, and, at the same time, it is used to fix the absolute level of the theoretical scattering curves. In a second step, we will try to fit the experimental dependence of $I(q \rightarrow 0)$ (and ξ) on λ, with the theoretical predictions. Since two of the approaches considered in paragraph 2 are based on elasticity theories, it is tempting to assume that they better describe the variation with λ of the macroscopic quantities, such as $I(q \rightarrow 0)$, rather than the "mesoscopic" ones, such as ξ. Finally, at the end of this section, the variation of $I(q)$ with q is investigated, the parameters obtained in the two first steps being maintained constant.

Let us discuss each model separately. Consider first the cluster model, which inspired this study. Actually, in a previous work, it was shown that the cluster model describes satisfactorily the small-angle neutron scattering from some swollen gels.[14] It was found that the variation of ξ and $I(q \rightarrow 0)$ with polymer volume fraction, ϕ (for $\lambda = 1$), can be described by power-laws, as proposed by the model. The exponents of the power-laws depend on the cross-link concentration ϕ_x (and probably on the preparation polymer volume fraction, ϕ_0). In particular, it was shown that for a statistical gel cross-linked at $\phi_0 = 0.1$, with a cross-linking ratio of $\phi_x = 0.8\%$ (the same as the present samples), the dependence of ξ_{gel} and $I_{gel}(q \rightarrow 0)$ on ϕ are quantitatively very close to the model predictions. Hence, we will skip the investigation of the dependence of $I(q \rightarrow 0)$ on ϕ for this model.

In Figure 5, $I(q \rightarrow 0)$ is plotted as a function of λ for both swelling ratios studied, together with the predictions of the theoretical models. It is observed in these figures that, for both swelling ratios, $I_{par}(q \rightarrow 0)$ increases strongly with the elongation ratio, λ, while $I_{per}(q \rightarrow 0)$ diminishes smoothly. If one fits the variation of $I_{par}(q \rightarrow 0)$ with λ as a power-law, one finds the exponent $\sim$2.1 for $Q = 12$, and 1.8 for $Q = 23$, instead of the exponent 8 predicted by the cluster model. For the variation of $I_{per}(q \rightarrow 0)$ with λ, much weaker exponents are found: -0.3 for $Q = 12$ and -0.56 for $Q = 23$, instead of -4 predicted by the model. All exponents are summarized in Table 2. Note that butterfly patterns are rather a result of the increase of the scattering

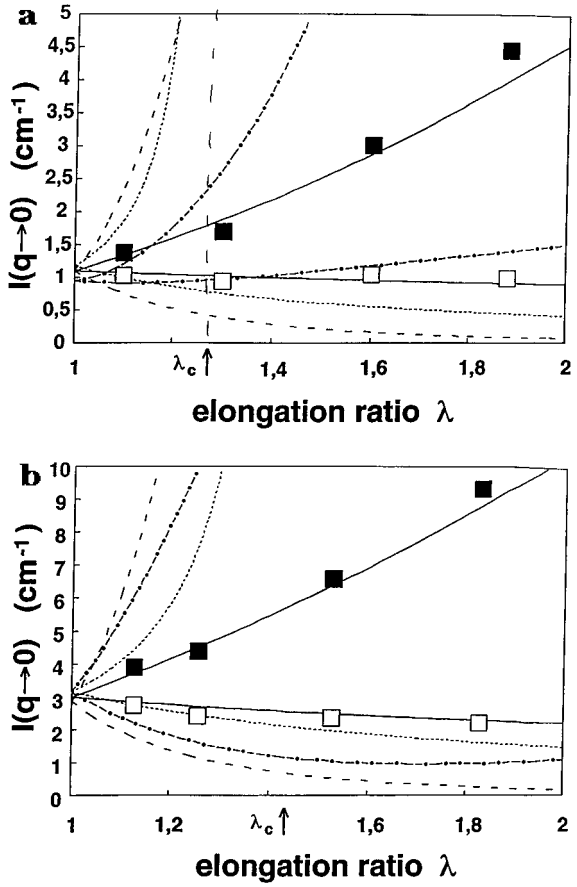

Figure 5. Scattered intensity extrapolated to zero wavevector, $I(q \rightarrow 0)$, as a function of elongation ratio, λ. Fittings derived from the different theoretical models are also shown: (- - - -) heterogeneous model; (— • —) thermal heterogeneous model; (•••••) strain concentration coupling model. The experimental scaling-law is (—). Two swelling ratios are considered: (a) $Q = 12$; (b) $Q = 23$. The position of the critical elongation ratio of the strain—concentration coupling model, λ_c, obtained from the fit, is also indicated.

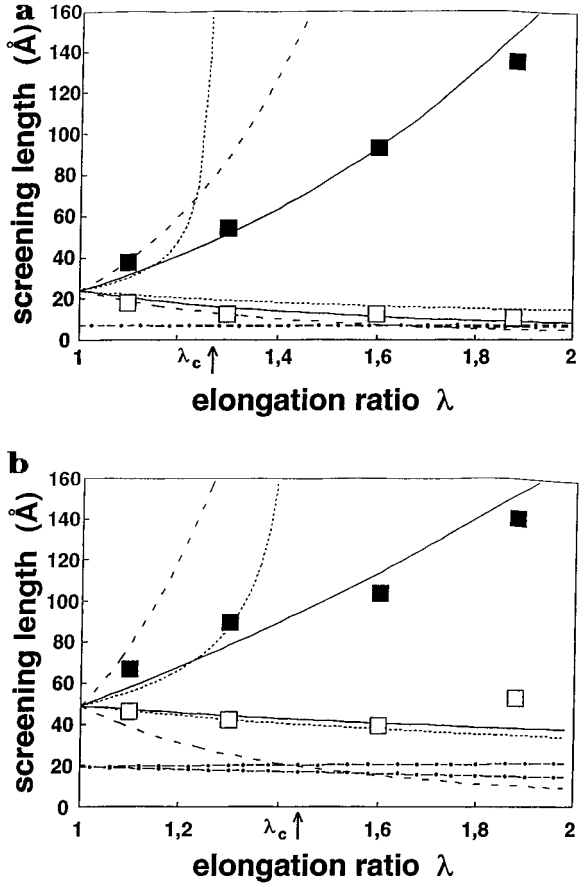

Figure 6. Experimental screening length, ξ, as a function of elongation ratio, λ. Fittings derived from the different theoretical models are also shown: (- - - -) heterogeneous model; (— • —) thermal heterogeneous model; (•••••) strain—concentration coupling model. The experimental scaling-law is represented by (—). Two swelling ratios are considered: (a) $Q = 12$; (b) $Q = 23$. The position of the critical elongation ratio of the strain—concentration coupling model, λ_c, obtained from the fit, is also idicated.

intensity in the direction parallel to the elongation direction than of a suppression of the scattering in the perpendicular direction.

In Figure 6, the values of ξ in the parallel and perpendicular directions are plotted as a function of λ. For $Q = 12$, we find $\xi_{par} \sim \xi_{iso}\lambda^{3.1}$. It is important to stress that the variation between ξ_{iso} and the first point ξ ($\lambda = 1.17$) is even stronger. On the other hand, for stronger elongation ratios, the apparent slope dimishes. In the perpendicular direction, the absolute variation of ξ_{per} with λ is smaller than that in the parallel direction: $\xi_{per} \sim \lambda^{-1.0}$ ($Q = 12$) and $\xi_{per} \sim \lambda^{-0.5}$ ($Q = 23$).

In summary, the same picture is found for the two studied concentrations with an increase in ξ and $I(q \rightarrow 0)$ with λ in the parallel direction and a decrease of these quantities in the perpendicular direction. At $Q = 23$, since the gel is more swollen, the initial isotropic values of ξ and $I(q \rightarrow 0)$ are greater than those found in the preceding case. As stressed above, the variation of such quantities (especially ξ) with ϕ in the relaxed state is very close to model predictions. However, the dependence of ξ and $I(q \rightarrow 0)$ on λ is much weaker than predicted. Following the picture presented in the model, this can be interpreted in terms of deformation of hard zones upon stretching. If such hard zones deform under uniaxial elongation, the separation in space, leading to an unscreening of correlations, should be much weaker than in the absence of deformation of heterogeneities.

Table 2. Exponents Obtained for the Quantities of Table 1, When the Scaling Laws, $\xi \sim \lambda^{\alpha}$ ξ_i and $I(q \rightarrow 0) \sim \lambda^{\beta}$ $I_i(q \rightarrow 0)$ Are Used for the Two Swelling Ratios Studied (The Index "*i*" Indicates the Isotropic State)

Q	$\alpha_{\|\|}$	$\alpha_{\perp}$	$\beta_{\|\|}$	$\beta_{\perp}$
12	3.09	−0.97	2.06	−0.30
23	1.62	−0.49	1.80	−0.56

Such a correction is not accounted for in the model which considers only anisotropic separation of hard zones when the system is elongated. This could also be the reason why no relation could be found between the exponents $\alpha_{\perp}$, $\alpha_{||}$, $\beta_{\perp}$, $\beta_{||}$. The relations recalled in paragraph 2 do not hold for the experimental values of these exponents.

Consider now Onuki's model. From equations 10, section 2, we can write the scattering intensity at the preparation concentration, $\phi = \phi_0$, for a gel in the relaxed state ($\lambda = 1$). This gives:

$$I_{\lambda=1,\phi=\phi_0}(q \rightarrow 0) = \frac{A}{\epsilon(\phi_0) + 1}\left(\frac{\phi_0}{\phi_x}\right) \qquad (19)$$

This equation is used in the determination of the constant A. For the statistical gels studied in the present work, it was shown previously[14] that the value of $I(0)_{\phi=\phi_0,\lambda=1}$ almost equals that of the solution prior to cross-linking. Hence, we find $A = 11.6$. The constant

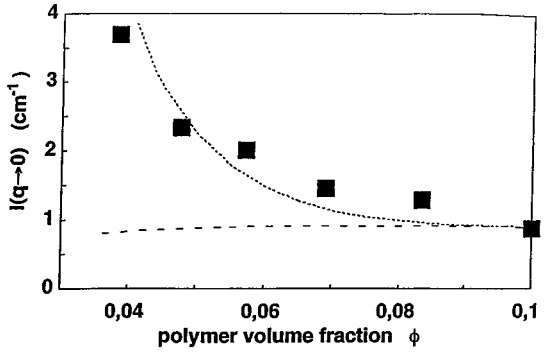

Figure 7. Scattered intensity extrapolated to zero wavevector, $I(q \rightarrow 0)$, as a function of polymer volume fraction, ϕ, in the absence of elongation. Fittings for the thermal heterogeneous model are plotted for different values of the parameter p: (- - - -) for $p = 0.01$ and (•••••) for $p = 30$.

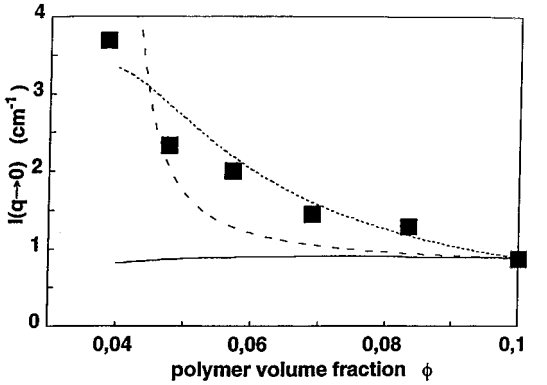

Figure 8. Same as Figure 7, with fittings for the strain−concentration coupling model. Different values of the parameter "a" are plotted: (—) for $a = 0.0$, (- - - -) for $a = 1.47$ and (•••••) for the law $a = a_0(\phi/\phi_0)^{2.65}$, with $a_0 = 12.5$.

p can be easily estimated if one considers the variation of $I(0)$ upon swelling in the relaxed case, $\lambda = 1$. In Figure 7, $I(0)$ is plotted as a function of ϕ (data from reference 14) together with the predictions of eq 10 for two values of the parameter p: 0.01 and 30. It can be seen that for $p \ll 1$, which should be a condition for the validity of the theory, that is, weak inhomogeneity, the model cannot account for the experimentally observed strong variation of $I(0)$ with ϕ. For this value of p, there is almost no variation of $I(0)$ with ϕ. In order to obtain an agreement between theory and experiment one should take $p \approx 30$, which is, in principle, not an allowed value.

Nevertheless, in order to investigate the dependence of $I(0)$ on λ, let us consider for the moment $p = 30$. This ensures a good starting value, $I(0)_{\lambda=1}$, for the two concentrations studied. In Figure 5, $I(0)$ is plotted as a function of λ. It can be seen from the figure that the theoretical variation is again, in the parallel direction, much stronger than the experimental variation. In the perpendicular direction, the discrepancy between experimental and theoretical predictions is much less important.

In summary, the variation of $I(0)$ with ϕ can be derived by Onuki's model provided that a very large value of the heterogeneity parameter, p, is imposed. This value exceeds the range of small perturbation, which is a basic assumption of the model. However, even with this large p value, the dependence of $I(0)$ on λ is much stronger than that observed experimentally. Since Onuki's model makes no provision for a variation of the correlation length with deformation, we will not discuss this quantity. It is noted in addition that Onuki's scattering function cannot be reduced to a Lorentzian form.

Consider now the Rabin−Bruinsma's model. As in the preceding discussion, one can easily determine the multiplicative prefactor, C_0, from the scattered intensity at $q \rightarrow 0$ in the preparation state:

$$I_{\text{prep}}(q \rightarrow 0) = \frac{C_0\phi_0^2}{\phi(\phi_0)} \tag{20}$$

where $f(\phi_0)$ is defined in eq 14.

Comparing expression 20 with the $I(q \rightarrow 0)$ data of reference 14, we find $C_0 = 540$.

Following the same procedure used above to determine the parameter p in Onuki's model, we will now analyze the dependence of $I(q \rightarrow 0)$ on ϕ for the swollen gels, for different values of $a(\phi)$. Remember that $a(\phi)$ is an unknown function of ϕ (see eq 14). In the swollen state, the gel is considered to be stretched in any direction to $\lambda = (\phi/\phi_0)^{-1/3}$. Thus, $I(q \rightarrow 0)$ can be written, from eq 16, as follows

$$I_{\text{iso}}(q \rightarrow 0) = \frac{C_0\phi^2}{f(\phi)}\left\{1 - \frac{2a(\phi)}{f(\phi)}[(\phi_0/\phi)^{1/3} - 1]\right\}^{-1} \tag{21}$$

Figure 8 shows the variation of $I(q \rightarrow 0)$ with ϕ as given by eq 21 for three different cases: $a(\phi) = 0$; $a(\phi)$ = constant, and $a(\phi) = a(\phi_0)\,(\phi/\phi_0)^{\delta}$. When $a(\phi) = 0$, we find the same behavior as for $p = 0$ in Onuki's model, that is, the scattered intensity remains approximately constant. For $a(\phi)$ = constant, that is, when $a(\phi)$ is only temperature dependent, the best agreement between theory and experiment is found for $a(\phi) = 1.47$. Nevertheless, such a variation cannot be considered as satisfactory. A much better agreement, is found when $a(\phi)$ is represented by a power-law dependence on concentration, that is, $a(\phi) = 12.5\,(\phi/\phi_0)^{2.64}$. The value of the exponent is completely empirical and it is not considered by the model.

Keeping this expression for $a(\phi)$, $I(0)$ and ξ are plotted as a function of λ in Figures 5 and 6. For the two swelling ratios studied, the theoretical predictions overestimate the measured values of $I(0)$ and ξ for different values of λ. In particular, this model predicts a divergence of the scattering function in the parallel direction for a critical value of the elongation ratio, $\lambda = \lambda_c$. One finds $\lambda_c = 1.28$ and 1.43 for $Q = 12$ and 23, respectively. Both values of λ_c are in the experimental range of λ used here. However, such a divergence, which is a direct consequence of the shape of the scattering function, is not observed experimentally.

As for the swollen polymers, it is instructive to measure the dependence of the parameter a on λ, in order to avoid the divergence, and to recover the experimental variation of $I(0)$ with λ. This is achieved as follows: comparing expression 16 for the intensity scattered in the parallel direction with the experimental data, we find the values of a, considering ϕ_0 as the reference state, that is, substituting λ in eq 16 with $\lambda(\phi/\phi_0)^{1/3}$.

Finally, consider the scattering intensity $I(q)$ in the parallel and perpendicular directions and its dependence on the elongation ratio, λ. As explained and discussed above, certain parameters of each considered theoretical model were fixed by studying the dependence of $I(q \rightarrow 0)$ on ϕ and ξ on the elongation ratio λ). For those fixed parameters, the best fittings for $I(q)$ should

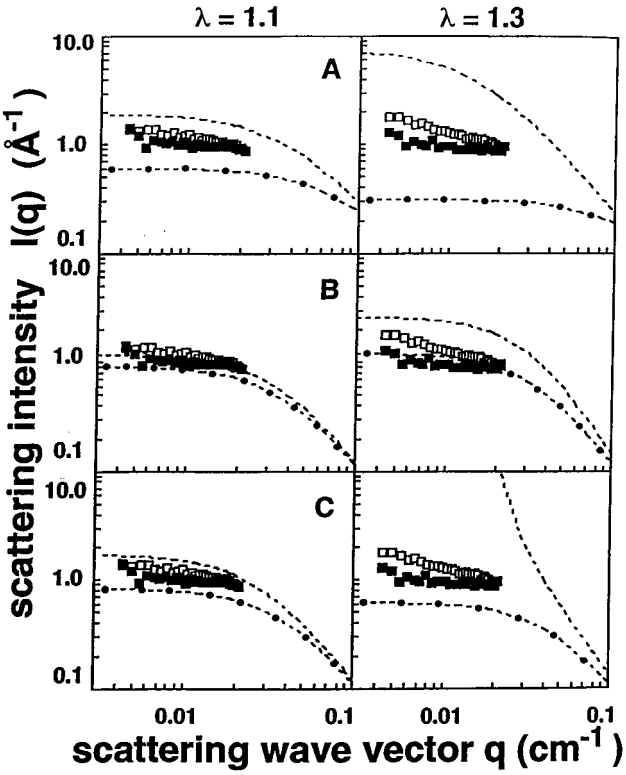

Figure 9. Scattered intensity in the parallel (q) and in the perpendicular (n) directions for the gel swollen to $Q = 12$. Two values of the elongation ratio, λ, are used: $\lambda = 1.1$ and $\lambda = 1.3$. The fittings for the three theoretical models considered in the text, in the perpendicular (- - - -) and in the parallel (− • −) directions are also plotted: (a) heterogeneous model; (b) thermal heterogeneous model; and (c) the strain−concentration coupling model.

be obtained for swelling ratios which are close to the preparation state and for small elongation ratios. In Figure 9, the scattered intensity is plotted as a function of the wave vector amplitude for two values of the elongation ratio, $\lambda = 1.1$ and $\lambda = 1.3$. The swelling ratio considered here is $Q = 12$, which is close to the preparation state, $Q_{prep} = 10$. The scattering functions determined using the theoretical models are shown in rows: (a) the cluster model; (b) the Onuki theory; (c) the Rabin−Bruinsma theory.

As before, the cluster model overestimates the intensity change. Such a disagreement could be a consequence of the deformation of the heterogeneities upon swelling or stretching, which is not considered by the model.

Consider row b of Figure 9, the Onuki theory predictions. The dependence of $I(q \rightarrow 0)$ on the elongation ratio, λ, is much closer to the experimental data than that found in row *a*, for this particular Q value and elongation ratio range. Nevertheless, the theoretical scattered intensity curve presents, at large q values, a dependence close to q^{-4} which has not been observed as yet. Experimental data in this scattering vector range ($q > 5\ 10^{-2}$ Å^{-1}; see Figure 4, $\lambda = 1.8$), suggest rather that $I(q)_{parallel} \sim q^{-\alpha}$, where $\alpha \approx 1.5$, which is significantly smaller than 4. In the perpendicular direction, such a dependence is even weaker.

Finally, in row c of Figure 9, data and fittings for the Rabin−Bruinsma model are plotted. For the smaller elongation ratio, the shape of the theoretical scattering function is very similar to the general form of the experimental scattering curves. However, for slightly higher elongation ratios, the theoretical curve diverges for a finite q value, which is not observed experimentally.

6. Summary and Conclusion

The small-angle neutron scattering spectra of uniaxially elongated swollen gels have been investigated as a function of the elongation ratio, λ, for two different polymer volume fractions, one very close to that of the preparation state and another close to the swelling equilibrium in a good solvent. An increase in intensity is observed at small angles in the direction parallel to the elongation axis, together with a decrease in the scattered intensity in the perpendicular direction. The combination of these two effects gives rise to the formation of isointensity curves in the form of "butterflies" on a bidimensional detector. The butterfly patterns become more pronounced as the elongation ratio increases. Such scattering patterns cannot be explained by classical rubber theories. However, the experimental data were compared with three recent theoretical models which, at least qualitatively, predict this behavior. In order to be able to perform a quantitative comparison, the scattering intensity was measured as a function of the elongation ratio, λ, in the directions parallel and perpendicular to the elongation axis. One obtained the extrapolated intensity to zero wave-vector, $I(q \rightarrow 0)$, and a screening length, ξ, as a function of the elongation ratio for the two principal directions. The dependence of these quantities on the elongation ratio, was compared to the predictions of the theoretical models, namely (i) the cluster model, (ii) the Onuki model, and (iii) Rabin−Bruinsma model.

For the type of "statistical" gels studied here, model i, which describes the network as containing fractal hard clusters was previously shown to describe well the variation of $I(q \rightarrow 0)$ as a function of the swelling ratio and the dependence with q of the scattering in the intermediate q range. However, the exponents, which were reported in this paper for the dependence of $I(q \rightarrow 0)$ and ξ with λ, are weaker than those proposed by the model in which the stretching of the clusters was ignored. Taking into account explicitly a cluster elongation would reduce the proposed "unscreening" of correlations in the parallel direction. It might a pathway for a better description of the data keeping the framework of a cluster model.

Using the Onuki model, which analyzes in a different manner the effects of the network heterogeneity, one can quantitatively fit the isotropic data at low q's, for different swelling ratios, provided a large amplitude of spatial fluctuations of cross-link points in space is considered, that is, for the heterogeneity parameter $p \sim 30$. But for this p value, the condition of small perturbation, considered in the development of the scattering function, is not respected anymore. Keeping $p = 30$, the theoretical dependence of $I(q \rightarrow 0)$ on λ was found to be stronger than the experimental one.

The Rabin−Bruinsma theory is entirely different since it does not consider any network heterogeneity. This model can also be used to fit the isotropic data, at different swelling degrees, provided a suitable choice is made for the dependence with volume fraction, ϕ, of the strain−concentration coupling parameter, $a(\phi)$. Keeping $a(\phi)$ found for the isotropic case, the model describes approximately the data for very small extension ratios λ. However, it predicts a unobserved divergence of the

scattering intensity for values of λ ($\sim$1.3) well below than the maximum elongation ratio. Such a disagreement is not fully conclusive since the theory is valid only for very small λ's.

In summary, these three models predict qualitatively the general features of the experimental data, for very small uniaxial deformations. However, at present, none of these models is able to describe quantitatively the large range of extension ratios. Once agreement is found for the swelling, the effects of elongation are overestimated by all the models. Therefore, from these data considered alone, it is hard to rule out any of these models and thus to discriminate unambiguously between the explanations based on structural heterogeneities and the hypothesis of coupling between thermal concentration fluctuations and strain. However, if one considers the larger ensemble formed by the present work and those reported in references 7−10, 14, 20, 21 the effect of static fluctuations coupled to structural inhomogeneities appears to be dominant. Comparisons to new theories (ref 24) and investigation of the structure by complementary techniques remain to be done.

References and Notes

(1) Benoît, H.; Higgins, J. *Polymer and Neutron Scattering*; Clarendon Press: Oxford, 1994.
(2) Boué, F. *J. Phys. (Paris)* **1982**, *43*, 137.
(3) Boué, F. *Adv. Polym. Sci.* **1987**, *82*, 47.
(4) Doi, M.; Edwards, S. F. *The Theory of Polymer Dynamics*; Clarendon Press: Oxford, 1986.
(5) Bastide, J.; Buzier, M.; Boué, F. *Polymer Motions in Dense Systems*; Richter, D., Springer, T., Eds.; Springer: Berlin, 1988.
(6) Boué, F.; Bastide, J.; Buzier, M. *Molecular Basis of Polymer Networks*; Baungärtner, A., Picot, C., Eds.; Springer: Berlin, 1989; p 65.
(7) Zielinski, F.; Buzier, M.; Lartigue, C.; Bastide, J.; Boué, F. *Prog. Colloid Polym. Sci.* **1992**, *90*(1), 111.
(8) Ramzi, A.; Zielinski, F.; Bastide, J.; Boué, F. *Macromolecules* **1995**, *28*, 3570−3587.
(9) Hayes, C.; Bokobza, L.; Boué, F.; Mendes, E.; Monnerie, L. *Macromolecules* **1996**, in press.
(10) Oeser, R. *Molecular Basis of Polymer Networks*; Baungärtner, A., Picot, C., Eds.; Springer: Berlin, 1989; p 65.
(11) Bastide, J.; Leibler, L. *Macromolecules* **1988**, *21*, 2647.
(12) Bastide, J.; Leibler, L.; Prost, J. *Macromolecules* **1990**, *23*,1821.
(13) Bastide, J.; Mendes, E.; Boué, F.; Buzier, M.; Lindner, P. *Makromol. Chem., Makromol. Symp.* **1990**, *40*, 81.
(14) Mendes, E.; Lindner, P.; Buzier, M.; Boué, F.; Bastide, J. *Phys. Rev. Lett.* **1991**, *66*(12), 1595.
(15) Onuki, A. *J. Phys. Soc. Jpn.* **1989**, *58*(9), 3065.
(16) Onuki, A. *J. Phys. II (Paris)* **1992**, *2*, 45.
(17) Panyukov, S. V. *Zh. Eksp. Teor. Fiz.* **1993**, *103*, 1287.
(18) Rabin, Y.; Bruinsma, R. *Europhys. Lett.* **1992**, *20*(1), 79.
(19) Bastide, J.; Boué, F.; Oeser, R.; Mendes, E.; Zielinski, F.; Buzier, M.; Lartigue, C. *Mat. Res. Soc. Symp. Proc.* **1992**, *248*, 313.
(20) Mendes, E.; Schosseler, F.; Isel, F.; Boué, F.; Bastide, J.; Candau, S. J. *Europhys. Lett.* **1995**, *32*(3), 273.
(21) Rouf, C.; Bastide, J.; Pujol, J. M.; Schosseler, F.; Munch, J. P. *Phys. Rev. Lett.* **1994**, *73*, 830.
(22) Bastide, J.; Candau, S. J. In *Physical Properties of Polymeric Gels*; Cohen-Addad, J. P., Ed.; J. Wiley: New York, 1996.
(23) Boué, F. In *Molecular characterisation of polymer networks*; Mark, J., Ed.; Oxford University Press: Cary, NC, 1996, in press.
(24) Panyukov, S. V.; Rabin, Y. *Phys. Rep.* **1996**, *269*, 1.
(25) Tanaka, T.; Hocker, L.; Benedek, G. *J. Chem. Phys.* **1973**, *59*, 5151.
(26) Mendes, E. Thesis, Université Louis Pasteur, Strasbourg, 1991.
(27) In reality, the system presents two gel points. One is the percolation gel point of blobs, related to the existence of one cluster containing frozen blobs that percolates. The second one, which is related to the gel point of the physical system in the vessel. Since the chains are considered to be long enough, one chain passes trough many different clusters of frozen blobs. Thus, for a sufficiently cross-linked system one finds a "real" gel far below the gel point of the blobs.
(28) de Gennes, P. G. *Scaling Concepts in Polymer Physics*; Cornell University Press: Ithaca, N.Y., 1979.
(29) Horkay, F.; Hecht, A. M.; Mallam, S.; Geissler, E.; Rennie, A. R. *Macromolecules* **1991**, *24*, 2896.
(30) Bastide, J.; Duplessix, R.; Picot, C.; Candau, S. J. *Macromolecules* **1984**, *17*, 83.
(31) Bruinsma, R.; Rabin, Y. *Phys. Rev. E* **1994**, *49*, 554.
(32) Collete, C.; Lafuma, F.; Audebert, R.; Leibler, L. In *Biological and Synthetic Polymer Networks*; Kramer, O., Ed.; Elsevier: Amsterdam, 1988; p 277.
(33) Benoît, H.; Picot, C. *Pure Appl. Chem.* **1966**, *12*, 545.

MA960043T